

# Comparative Analysis of Strain Fields in Step-graded Buffers of Different Design, based on $\text{In}_x\text{Al}_{1-x}\text{As}$ Ternary Solutions

Aleshin AN<sup>1</sup>, Bugaev AS<sup>1</sup>,  
Ruban OA<sup>1</sup>,  
Shchetin IV<sup>2</sup> and  
Tabachkova N.YU<sup>2</sup>

## Abstract

Two heterostructures with the step-graded buffers of different design grown on (001) GaAs substrates by molecular beam epitaxy were employed to reveal applicability of an extension of phenomenological approach developed for the description of strain relief in single layer hetero structures to multilayer thin film systems. Difference in the design of buffers provided to the formation of dislocation free layers of different thickness. The determination of the residual strains in the epitaxial layers was done using reciprocal space mapping performed with a triple-axes X-ray diffractometer Smart Lab 9kW and the following processing of data obtained within the linear theory of elasticity. It was established that, despite the different design of buffers the character of strain spatial distributions in them was similar. It gives possibility to attract a phenomenological rule to describe the strain relief in the final constructive elements of both hetero structures. A correction for a work hardening in the phenomenological rule governing the strain relief in single layer heterostructures was performed.

**Keywords:** Triple-axes X-ray diffractometry; Reciprocal space mapping; Elastic strain; Step-graded buffer, Spatial strain distribution; Work hardening

- 1 Institute of Ultrahigh Frequency Semiconductors Electronics, Russian Academy of Sciences, Moscow, Russian Federation.
- 2 National University of Science and Technology "MISIS" Moscow, Russian Federation.

**Corresponding author:** Aleshin AN

✉ a.n.aleshin@mail.ru

Institute of Ultrahigh Frequency Semiconductors Electronics, Russian Academy of Sciences, Moscow, Russian Federation.

**Tel:** +79166341440

**Received:** November 30, 2016; **Accepted:** February 03, 2017; **Published:** February 05, 2017

## Introduction

Hetero structures applied to ultrahigh frequency (UHF) electronics devices (for example, high electron mobility transistors–HEMTs) are created, as a rule, on a single crystal substrate GaAs of (001) orientation and consist of a metamorphic (MM) buffer aiming to remove a mismatch between the substrate and device active layers including a quantum well (QW). The MM-buffer may have a different design, for example, it may be step-graded [1-3] or linear graded with an increasing value of the lattice misfit [2,3]. Very often, the MM-buffer has such additional elements as a healing layer or an inverse step [4]. During the successive growth of MM-buffer layers, the strain relief occurs, which is accompanied by the generation of misfit dislocations and the propagation of threading dislocations into heterostructure top layers [5]. The MM-buffer should prevent the penetration of threading dislocations into the device active layers. The creation of MM-buffer is based on possibility of the system to form a dislocation free layer, which is, in its turn, a platform for following the healing layer or the inverse step. The theoretical prediction of the formation of such a dislocation free layer was done in [6]

This model considered MM-buffer with a continuous increasing lattice misfit due to the increase of the concentration of an alloying element. When moving this system to the equilibrium, the formation of dislocation free layer at the top region of buffer gives an energetic gain for the system [3-6]. Details concerning the mechanism of strain relief are currently revealed for single heteroepitaxial layers. It was established that there are three stages of strain relief [7]. In the first one, the process of relaxation is slow because only the bending of the dislocations penetrating from the substrate to the epitaxial layer takes place. The second stage of relaxation is the fast stage due to the multiplication of misfit dislocations; this stage occurs if the thickness of layer is more than 100 nm. The third stage manifests an inhibition of dislocation multiplication and occurs for much thicker layers due to the work hardening. For the fast stage of strain relief, there are some numerical relations between a residual strain and a thickness of single heteroepitaxial layer. Thus, Dunstan with

collaborators in the series of articles [8-10] gave some evidence concerning the existence of an inverse proportion between the residual compressive strain and the layer thickness of 100-1000 nm. Such a relation between strains and thicknesses was explained in the framework of a “geometrical approach” taking into account the character of the spatial distribution of misfit dislocations in the region between the substrate and the growing epitaxial layer. By contrary, in [11] there was established that the residual compressive strain varies in an inverse proportion to the root square of layer thickness. It means that there is an energetic limit for an elastic strained thin film, which governs the strain relief in single layer hetero structures. Both these approaches may be described numerically and each of them is characterised by its own phenomenological constant. Such a description of strain relief in single layer hetero structures may be considered as a phenomenological approach. This article is aimed to reveal possibility of the application of the phenomenological approach to describe the strain relief in multilayer systems, particularly, in MM step-graded buffers, and to find some numerical criterions for the formation of dislocation free layer. We believe that the comparative analysis of the structural parameters of step-graded MM-buffers of different design is a key to solve this problem. Two step-graded MM-buffers of different design are the subjects of this investigation. The principle difference between two MM-buffers concluded in their final constructive elements: first of them was terminated by the healing layer and second one had in its structure the inverse step. Moreover, the buffers had different thicknesses of their steps. The epitaxial layers of both step-graded MM-buffers were based on  $\text{In}_x\text{Al}_{1-x}\text{As}$  ternary solid solutions. X-ray reciprocal space mapping and transmission electron microscopy (TEM) were involved in this study. Below, the hetero structures with MM-buffers we will mark as metamorphic HEMTs – MHEMTs.

## Experimental

### Sample preparation

Molecular beam epitaxy (MBE) was employed to create two MHEMTs with the step-graded buffers of different design. A

Riber 32 MBE system was used for the fabrication of MHEMTs. MHEMTs consisted of  $\text{InAlAs}/\text{InGaAs}/\text{InAlAs}$  active layers and six-layered MM-buffers. The layers covering up the upper steps of MM-buffers, the healing layer (MHEMT 1) or the inverse step (MHEMT 2), had close values of the molar fraction of In. In these constructive elements of MHEMTs the molar fraction of In,  $X_{\text{In}}$  was equal to 0.39 and 0.394, correspondingly. MBE was performed at a constant temperature of substrates. MHEMT 1 was grown on a standard semi-isolated (001) GaAs substrate, while MHEMT 2 was grown on the vicinal surface of GaAs substrate with a deviation angle of  $2^\circ$  from (001) plane. The step-to-step change in the molar fraction of In in  $\text{In}_x\text{Al}_{1-x}\text{As}$  ternary solutions for the first five steps of MM-buffers was achieved in the process of non-interrupted epitaxial growth at a constant Al-source temperature. At this stage of heterostructure growth, the thickness of each layer was equal to 0.1  $\mu\text{m}$  for MHEMT 1 and 0.2  $\mu\text{m}$  for MHEMT 2. During growth, the temperature of substrates was equal to 380°C for MHEMT 1 and 400°C for MHEMT 2. The barriers layers of both MHEMTs were grown at the higher temperatures of the substrates: 480 and 500°C, correspondingly. The growth rate of epitaxial layers was equal to 0.5  $\mu\text{m}/\text{h}$ . The layer by layer growth was interrupted for two minutes prior to the growth of the healing layer (MHEMT 1) or the inverse step (MHEMT 2). The growth was also interrupted for five minutes when transiting to the regime of high temperature growth. The composition of the epitaxial layers was controlled by regulating the temperature of In, Al, Ga, as and Si molecular sources based on the calibrated temperature dependence of molecular fluxes. The common feature of two MHEMTs was the equality of thicknesses of the final constructive elements: the healing layer (MHEMT 1) and the inverse step (MHEMT 2). The thicknesses of the barriers layers in both MHEMTs were also equal. The details concerning the process of epitaxial growth and the technological characteristics of the constructive elements of MHEMTs are presented in Table 1 X-ray diffraction measurements were performed with a Smart Lab 9 kW X-ray diffractometer in the three-axial configuration. The diffractometer operated in the step-by-step mode of X-ray recording using the  $\text{Cu K}_{\alpha(1)}$

**Table 1** The main parameters of the growth of MHEMT epitaxial layers.

MHEMT	Layer number	$X_{\text{In}}$	Layer thickness, $\mu\text{m}$	Layer destination	Substrate temperature, $^\circ\text{C}$
1	1	0.15	0.1	First step of buffer	380
	2	0.23	0.1	Second step of buffer	380
	3	0.29	0.1	Third step of buffer	380
	4	0.35	0.1	Fourth step of buffer	380
	5	0.39	0.1	Fifth step of buffer	380
	6	0.39	0.2	Healing layer	380
	7	0.39	0.2	Barrier layer	480
2	1	0.10	0.2	First step of buffer	400
	2	0.20	0.2	Second step of buffer	400
	3	0.30	0.2	Third step of buffer	400
	4	0.39	0.2	Fourth step of buffer	400
	5	0.48	0.2	Fifth step of buffer	400
	6	0.394	0.2	Inverse step	400
	7	0.394	0.2	Barrier layer	500

irradiation. A Ge single crystal with (002) orientation was employed as an analyzer crystal. Two reflections, 004 and 224 (at glancing exit geometry), were recorded in the regime of the so-called  $\omega$ - $2\theta$  scanning, which implies the use of Bragg – Brentano technique with the variation of sample position relatively the Bragg maximum of substrate. During recording, X-ray reflected radiation was detected along the scattering vector  $H_{hkl}$ ;  $H_{001}$  (for symmetric recording) and  $H_{224}$  (for asymmetric recording). The initial position for 004 symmetric recording corresponded to the Bragg maximum of the substrate ( $\Omega=\delta$ ), where  $\omega$  is a deviation of the substrate from the Bragg position). Such a mode of recording allowed us to reveal minor X-ray maxima for all layers of MM-buffers. For asymmetric recording, the scanning along the scattering vector  $H_{224}$  is achieved by the variation of hkl values that gives the decomposition of the scattering vector  $H_{224}$  along the directions [001] and [110] of the reciprocal space. On the basis of the  $\omega$ - $2\theta$  scanning, it is possible to plot the so-called reciprocal space maps, which represent the positions of minor X-ray maxima in the reciprocal space. The use of the technique of reciprocal space mapping have some advantages in comparison with the conventional technique of rocking curves because the latter is invalid in the case of the spatial disorientation of epitaxial layers relative the substrate. The effect of spatial disorientation between an epitaxial layer grown on the vicinal surface of substrate and the corresponding substrate plane is a well-known fact [12]. The angular parameters of spatial disorientation of epitaxial layers in heterostructures grown on the vicinal surface of (001) GaAs substrate were presented in [12,13,14]. The actual axes of reciprocal space for epitaxial films grown on (001) GaAs substrates are the axis [110] (axis Y) and the axis [001] (axis Z). The antinodes of iso-concentration contours revealed in the reciprocal space maps correspond to the interference maxima of X-ray radiation. The coordinates of the antinodes (X-ray maxima) are expressed by the vectors  $q_{110}$  and  $q_{001}$ , which are deviations (along the corresponding reciprocal space axes) of minor X-ray maxima from the major X-ray maximum  $H_{wd}^0$  corresponding to the substrate. The knowledge of  $q_{110}$  and  $q_{001}$  allows us to determine the vertical and lateral lattice parameters for all epitaxial layers.

### Characterization of MHEMTs microstructure

The structural investigation of MHEMTs was performed by TEM with a Jeol JEM-2100 operating at an accelerating voltage of 200 kV Figure 1 shows cross-sectional bright-field electron microscopy images obtained for two investigated MHEMTs. It is seen that, despite the interruption of growth, layers 5, 6 and 7 in MHEMT 1 do not have interphase boundaries and we can consider them as a single phase. This combined layer of MHEMT 1 does not have threading dislocations and, consequently, the elastic strain developed in it should be sufficiently higher than that in the internal layers of MHEMT 1. Similar situation, the formation of dislocation free layer, is realized for layer 5 in MHEMT 2. The inverse step and the barrier layer of this MHEMT (layers 6 and 7) are the special elements of heterostructure design; similar layer 5 these layers do not have threading dislocations. The role of these constructive elements in the formation of strain fields in MHEMT 2 will be discussed below. It is important that, the

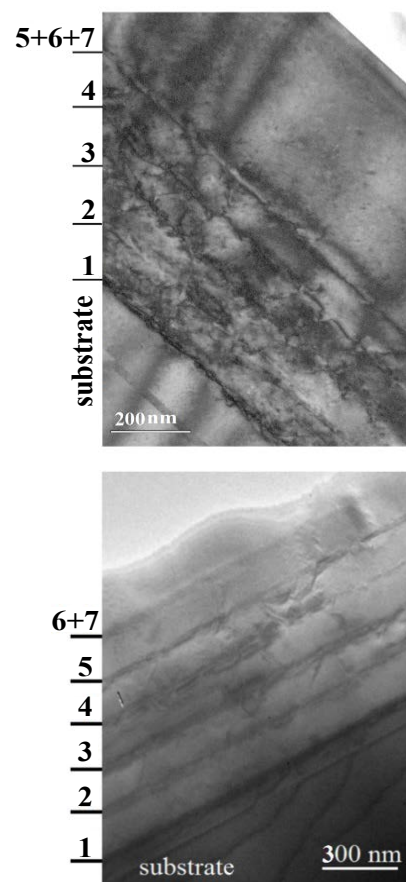
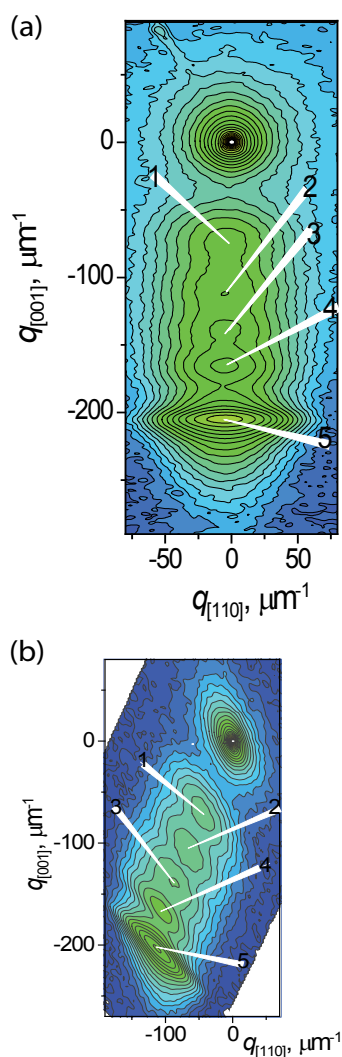


Figure 1 The cross-sectional bright field images for (a) MHEMT 1 and (b) MHEMT 2.

electron microscopy image taken from MHEMT 2 demonstrates the inverse step and the barrier layer as a single structural layer.

### Reciprocal space maps and their processing

Reciprocal space maps for MHEMTs under study plotted on the basis of 004 and 224 reflections are presented in Figure 2 (MHEMT 1) and Figure 3 (MHEMT 2). The maps for MHEMT 1 manifest five minor X-ray maxima whose values of  $|q_z|$  (in ascending order) correspond to layers 1, 2, 3, 4 and 5 (6, 7). Attention is drawn to the fact that layers 5, 6 and 7 are characterized by a single reflex that indicates the affinity of the structural parameters of these layers. The similar situation is realized for layers 6 (the inverse step) and 7 (the barrier layer) of MHEMT 2; these layers are also characterized by a single X-ray maximum. So, the reciprocal space maps are in agreement with the MHEMTs microstructure revealed by TEM. The arrangement of minor X-ray maxima in the reciprocal space maps for MHEMT 2 is more complicated than that for MHEMT 1 due to their partial overlap and absence of sharp X-ray maximum corresponding to layer 4. To find all positions of interference maxima in the map obtained for 004 reflection we use the procedure of the modelling of X-ray sans by a set of Gaussians [14]. Taking into account that for MHEMT 2 there is no a difference in microstructure between the inverse step and the barrier layer Figure 1b we considered the strong central X-ray peak at the reciprocal space maps for MHEMT 2



**Figure 2** The reciprocal space maps plotted for MHEMT 1 on the basis of (a) 004 reflection and (b) 224 reflection. The numerals indicate the number of layer responsible for the appearance of given X-ray maximum.

as the peak corresponding simultaneously to both constructive elements. This circumstance facilitates the processing of the map plotted on the basis of 004 reflection for MHEMT 2 (the expansion of X-ray scan along the axis Z on six Gaussians) and allows us to determine the values of  $q_z^{004}$  and  $q_y^{004}$  for layers 3, 4, and 6(7). For all maps the coordinates of distinct defined X-ray maxima, the values of  $q_y$  and  $q_z$  were determined by searching for the maximal value of X-ray reflected radiation counts using a special option of the Origin 15 software. The  $q_z^{004}$ ,  $q_y^{004}$ , and  $q_y^{224}$  values (excepting the value of  $q_y^{224}$  for layer 4 in MHEMT 2) are listed in Table 2. The complete characterization of the structural state of layer 4 in MHEMT 2 was done using the specific features of the MHEMT 2 arrangement and will be described below.

### Strain fields in epitaxial layers of MHEMTs

The vectors  $q_z^{004}$ ,  $q_y^{004}$ ,  $q_y^{224}$ , and allow us to determine the so called “total” strains (relative to GaAs substrate) of MHEMTs

epitaxial layers:  $[(a_{\perp} - a_s)/a_a]_{[001]}$  (based on 004 reflection) and  $[(a_{\perp} - a_s)/a_a]_{[001]}$  (based on 224 reflection), where  $a_{\perp}$  are, respectively, the vertical and lateral lattice parameters of layer and  $a_s$  is the substrate lattice parameters. In accordance with [15], for the epitaxial layers of MHEMTs created on GaAs substrates the “total” strains are determined by the following relationships.

$$\left(\frac{a_{\perp} - a_s}{a_s}\right)_{[001]} = -\frac{q_z^{004}}{4/a_s + q_z^{004}} \quad (1)$$

$$\left(\frac{a_{\perp} - a_s}{a_s}\right)_{[110]} = -\frac{Q_y^{224}}{2^{3/2}/a_s + Q_y^{224}}, \quad (2)$$

where

$$Q_y^{224} = q_y^{224} - q_y^{004}. \quad (3)$$

Eq. (3) takes into account the effect of spatial misorientation of epitaxial layers relative to the substrate. The quantities  $[(a_{\perp} - a_s)/a_a]_{[001]}$  and  $[(a_{\perp} - a_s)/a_a]_{[110]}$  correspond to the total strains  $\epsilon_{33}$  and  $\epsilon_{11}$ , which are directed along the main crystallographic axes. (Note, when rotating a cubic lattice by an angle of  $45^\circ$  about the axis [001, the required operation for transition from the axis [110] to the axis [100], the equality between the quantities  $[(a_{\perp} - a_s)/a_a]_{[110]}$  and  $\epsilon_{11}$  will be achieved, if the distortion tensor does not have off-diagonal components and the elastic strains  $e_{11}$  and  $e_{22}$  are equal. Generally, this condition is accepted default). The knowledge of the values of  $E_{33}$  and  $\hat{a}_{11}$  gives us possibility to calculate the lattice misfit  $E_0 = (a_r - a_s)/a_s$ , where  $a_r$  is the lattice parameter of fully relaxed lattice, and the residual compressive elastic strain  $\hat{a}_{11}$  on the basis of Hooke law using the linear theory of elasticity. The concept according to which the residual strain in epitaxial layers is elastic is conventional and generally accepted in calculations of the lattice misfit  $\epsilon_0$ . According to this concept, the stress  $\sigma_{33}$  in the [001] direction is assumed to be zero due to the plastic deformation near the interphase boundaries oriented perpendicular to the [001] axis. On the basis of the equality of lateral stresses  $\sigma_{11}$  and  $\sigma_{22}$ , it follows from the Hooke law for the crystals of cubic system, elastic strains  $e_{11}$  and  $e_{33}$  are subjected to the next relation

**Table 2** Reciprocal space vectors for the maps obtained on the basis of 004 and 224 reflections.

MHEMT	Layer	$q_z^{004}, \mu\text{m}^{-1}$	$q_y^{004}, \mu\text{m}^{-1}$	$q_y^{224}, \mu\text{m}^{-1}$
1	1	-75.36	-4.90	-44.93
	2	-111.45	--5.00	-67.39
	3	-139.32	-5.03	-86.96
	4	-165.35	-5.11	-110.07
	5 (6,7)	-204.70	-5.00	-111.71
2	1	-62.41	-5.20	-35.07
	2	-109.87	-5.20	-61.79
	3	-152.47	-4.63	-90.63
	4	-188.22	4.05	-
	5	-256.49	6.27	-120.66
	6 (7)	-179.00	6.27	-120.66

$$\frac{e_{33}}{e_{11}} = -\frac{2C_{12}}{C_{11}}, \quad (4)$$

where  $C_{11}$  and  $C_{12}$  are the elastic stiffness coefficients. The relationship between the total strains  $\epsilon_{ii}$  (measured directly in an experiment) and the elastic strain  $e_{11}$  is expressed by the following relationship [16]

$$e_{ii} = \hat{a}_{ii} - \hat{a}_0 \quad (5)$$

Taking into consideration Eq. (4) and Eq. (5) we arrive to

$$\hat{a}_0 = \hat{a}_{33} - \frac{2\tilde{N}_{12}}{\tilde{N}_{11} + 2\tilde{N}_{12}} (\hat{a}_{33} - \hat{a}_{11}) \quad (6)$$

The results of calculation of  $\hat{a}_0^{(n)}$  and  $e_{11}^{(n)}$  ( $n$  is the layer number)

based on the measured  $q_z^{004}$ ,  $q_y^{004}$  and  $q_y^{224}$  values are presented in Table 3. The GaAs lattice parameter was assumed to be 0.565321 nm [17]. The elastic stiffness coefficients  $C_{11}$  and  $C_{12}$  of  $\text{In}_x\text{Al}_{1-x}\text{As}$  ternary solutions, which must be known to calculate  $\hat{a}_0^{(n)}$  and  $e_{11}^{(n)}$  were obtained on the basis of the Vegard law proceeding from the corresponding data for AIAs and InAs [18]. For MHEMT 2 the values of  $\hat{a}_0^{(n)}$  and  $e_{11}^{(n)}$  were determined on the basis of a linear dependence of  $\epsilon_0$  on the layer position in space and using Eq. (6). Results presented in Table 3 allows us to conclude that the design of MM-buffer in MHEMT 2 satisfies the philosophy of the inverse step creation [4] because the strain in this constructive element of MM-buffer is practically equal to zero. The existence of the inverse step in MM-buffer of MHEMT 2 does not influence the strain field in the internal layers of the buffer. Because layers 6 and 7 of MHEMT 2 do not contribute the strains into the total strain field, they were excluded from the following analysis. The lattice misfit spatial profiles and strain spatial profiles in both MHEMTs are shown in Figures 4 and 5 correspondingly. The residual strain profiles in MHEMTs are presented in the form of a function of  $e_{11}$  on  $\epsilon_0$ . Both dependences are similar and manifest non-zero strains for the internal layers of MM-buffers that is in contradiction with the models predicting the full strain relief in internal layers [19,20]. Such a situation is realized due to the work hardening, which may appear in multilayer systems at sufficiently

less epitaxial layer thicknesses in comparison with a single layer heterostructure [20].

**Table 3** The lattice misfit, the residual strain and the thickness of the constructive elements of MM-buffers.

MHEMT	Layer	$\epsilon_0$	$\epsilon_{11}$	Constructive element thickness, $\mu\text{m}$
1	1	$9.444 \cdot 10^{-3}$	$-1.38 \cdot 10^{-3}$	0.1
	2	$14.342 \cdot 10^{-3}$	$-1.71 \cdot 10^{-3}$	0.1
	3	$18.385 \cdot 10^{-3}$	$-1.74 \cdot 10^{-3}$	0.1
	4	$22.686 \cdot 10^{-3}$	$-1.26 \cdot 10^{-3}$	0.1
	5 (6,7)	$25.801 \cdot 10^{-3}$	$-4.01 \cdot 10^{-3}$	0.5
2	1	$7.483 \cdot 10^{-3}$	$-1.48 \cdot 10^{-3}$	0.2
	2	$13.648 \cdot 10^{-3}$	$-2.21 \cdot 10^{-3}$	0.2
	3	$19.779 \cdot 10^{-3}$	$-2.29 \cdot 10^{-3}$	0.2
	4	$25.829 \cdot 10^{-3}$	$-1.51 \cdot 10^{-3}$	0.2
	5	$31.815 \cdot 10^{-3}$	$-5.78 \cdot 10^{-3}$	0.2
	6 (7)	$25.993 \cdot 10^{-3}$	$0.04 \cdot 10^{-3}$	0.4

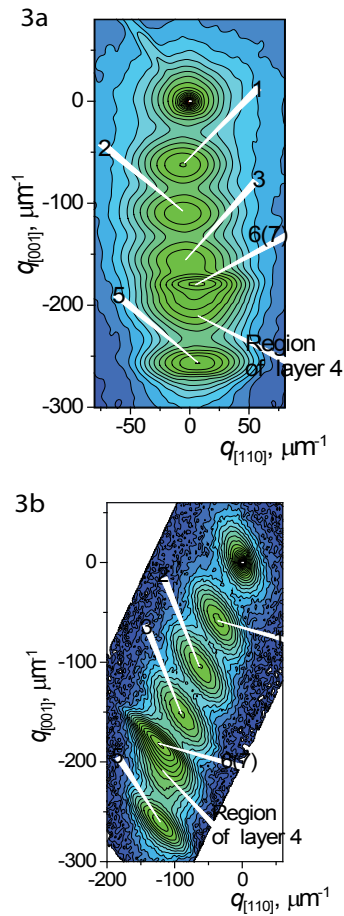


**Figure 3** The reciprocal space maps plotted for MHEMT 2 on the basis of (a) 004 reflection and (b) 224 reflection. The numerals indicate the number of layer responsible for the appearance of given X-ray maximum.

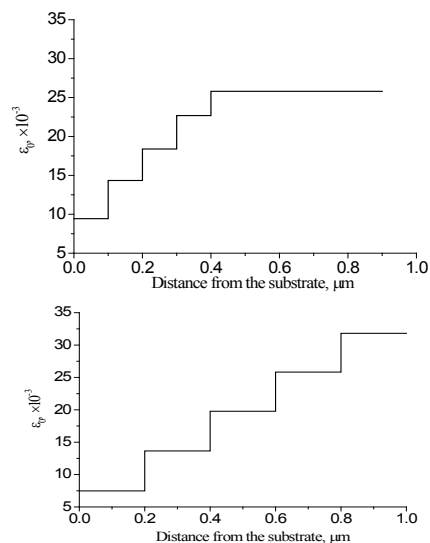


**Figure 4** The lattice misfit spatial profiles in the epitaxial layers of MM-buffers for: (a) MHEMT 1 and (b) MHEMT 2.

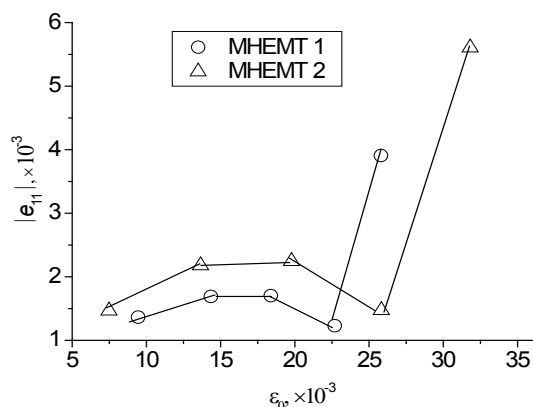


**Figure 5** The strain spatial distributions plotted in the form of a function of  $e_{11}$  on  $\epsilon_0$  for MHEMTs.

## Discussion

On the basis of our experimental data, it is possible to show that for two MHEMTs the following relationship is performed

$$\left[ \left( e_{11}^{(5-6-7)} - e_{11}^{(4)} \right)^2 h_{df} \right]_{\text{MHEMT 1}} = \left[ \left( e_{11}^{(5)} - e_{11}^{(4)} \right)^2 h_{df} \right]_{\text{MHEMT 2}} \quad (7)$$

where  $h_{df}$  is the thickness of the dislocation free layer. For MHEMT 1  $h_{df} = 0.5 \mu\text{m}$ ; for MHEMT 2  $h_{df} = 0.2 \mu\text{m}$ . Eq. (7) characterises numerically the process of strain relief in the final constructive elements of MM-buffer in MHEMTs. The product  $\left( e_{11}^{(5-6-7)} - e_{11}^{(4)} \right)^2 h_{df}$  equals 0.0038 nm while the product  $\left( e_{11}^{(5)} - e_{11}^{(4)} \right)^2 h_{df}$  is equal to 0.0036 nm. The average value of two products equals 0.0037 nm.

In a general form Eq. (7) can be written as

$$\left( e_{11}^{df} - e_{11}^{ial} \right)^2 = \frac{k}{h_{df}} \quad (8)$$

where  $e_{11}^{df}$  the residual strain in the dislocation free layer,  $e_{11}^{ial}$  is the residual strain in the internal adjacent layer and  $k$  is a phenomenological constant. Attention is drawn to the fact that Eq. (8) is very close to the equation describing the strain relief in a single layer heterostructure. As was shown in [11], the strain relief of epitaxial layer of In Ga As grown on (001) GaAs substrate is governed by the equation

$$e_{11}^2 = \frac{k}{h} \quad (9)$$

where  $h$  is the thickness of epitaxial layer. The phenomenological constant  $k$  in Eq. (9) is equal to 0.0037 nm. Eq. (8) and Eq. (9) operate equal values of  $k$  that indicates the common mechanism of strain relief in both cases. We may consider Eq. (8) as an extension of Eq. (9) to two layer thin film system where the dislocation free layer plays the role of a substrate. It should be pointed out that, in such a two layers system the strain relief occurs in the internal layer while the dislocation free layer exhibits strong compression. Because the dislocation free layer is sufficiently thinner than a real massive substrate in a single layer heterostructure, it gives a possibility to perform its pseudomorphic growth on the platform of internal adjacent layer. Both layers, the dislocation free layer and the internal adjacent layer, are, in fact, the single equalized system. The determination of interrelations between residual strains in all the layers of multilayer system requires additional investigation.

## Conclusion

The performed study gives some evidence concerning the possibility of numerical description of a value of strain in the dislocation free layer of the step-graded MM-buffer in the framework of the phenomenological approach developed for single layer hetero structures. This description has a quadratic form as an inverse proportion between the residual compressive strain in the dislocation free layer and the root square of the layer thickness. The value of the phenomenological constant governing the process of the strain relief in the layers of metamorphic step-graded buffers based on ternary  $\text{In}_x\text{Al}_{1-x}\text{As}$  solutions coincides with that which controls the strain relief in single layer hetero structures. The numerical expression takes into account a correction for the work hardening in the internal layer adjacent to the dislocation free layer.

## Acknowledgement

The reported study was partially funded by Russian Funding for Basic Research according to the research projects

No№ 16-32-00552 mol\_a, 16-07-00187 A, 17-32-80009 mol\_ev\_a, 16-29-03033 ofi\_m.

## References

- 1 Imaizumi M, Hirotani M, Soga T (2015) Study on Effect of an Intermediate Buffer Layer Structure on the Growth of GaAs Layers on GaP Substrates. 42 IEEE Photovoltaic Specialist Conference.
- 2 Kumar R, Bag A, Mukhopadhyay P, Das S, Biswas D (2015) Comparison of different grading schemes in InGaAs metamorphic buffers on GaAs substrate: Tilt dependence on cross-hatch irregularities. Applied Surface Science 357: 922-930.
- 3 Kujofsa T, Ayers JE (2015) Equilibrium lattice relaxation and misfit dislocations in continuously- and step-graded  $\text{In}_x\text{Ga}_{1-x}\text{As}/\text{GaAs}$  (001) and  $\text{GaAs}_{1-y}\text{P}_y/\text{GaAs}$  (001) metamorphic buffer layers. International Journal of High Speed Electronics and Systems 24: 1-8.
- 4 Galiev GB, Klimov EA, Imamov RM, Ganin GV (2016) High-resolution X-ray diffractometry and transmission electron microscopy as applied to the structural study of InAlAs/InGaAs/InAlAs multilayer transistor nano heterostructures. Journal of Surface Investigation, X-ray Synchrotron, and Neutrons Techniques 10: 495-509.
- 5 Ayers JE (2007) Heteroepitaxy of semiconductors theory growth and characterization. Taylor and Francis Group.
- 6 Tersoff J (1993) Dislocations and strain relief in compositionally graded layers. Appl Phys Lett 62: 693-695.
- 7 Dunstan DJ (1997) Strain and strain relaxation in semiconductors. J Mater Sci: Mater Electronics 8: 337-375.
- 8 Dunstan DJ, Young S, Dixon RH (1991) Geometrical theory of critical thickness and relaxation in strained-layer growth. J Appl Phys 70: 3038-3045.
- 9 Dunstan DJ, Kidd P, Howard LK, Dixon RH (1991) Plastic relaxation of InGaAs grown on GaAs. Appl Phys Lett 59: 3390-3392.
- 10 Dunstan DJ, Kidd P, Fewster PF, Andrew NL (1994) Plastic relaxation of metamorphic single layer and multilayer InGaAs/GaAs structures. Appl Phys Lett 65: 839-841.
- 11 Drigo AV, Aydinli A, Carnera A (1989) On the mechanisms of strain release in molecular beam epitaxy grown InGaAs/GaAs single heterostructures. J Appl Phys 66: 1975-1983.
- 12 Ayers JE, Ghandhi SK, Schowalter LJ (1991) Crystallographic tilting of heteroepitaxial layers. J Cryst Growth 113: 430-440.
- 13 Lee D, Park MS, Tang Z (2007) Characterization of metamorphic  $\text{In}_x\text{Al}_{1-x}\text{As}/\text{GaAs}$  buffer layers using reciprocal space mapping. J Appl Phys 101: 063523.
- 14 Aleshin AN, Bugaev AS, Ermakova MA (2015) Study of a MHEMT heterostructure with an  $\text{In}_{0.4}\text{Ga}_{0.6}\text{As}$  channel MBE-grown on a GaAs substrate using reciprocal space mapping. Semiconductors 49: 1039-1044.
- 15 Chauveau JM, Androussi Y, Lefebvre A (2003) Indium Content measurements in metamorphic high electron mobility transistor structures by combination of X-ray reciprocal space mapping and transmission of electron microscopy. J Appl Phys 93: 4219-4225.
- 16 Khapachev YP, Dyshenkov AA, Kiselev DS (1984) The theory of X-ray diffraction analysis of elastic-strain states in epitaxial films. Phys Stat Sol B 126: 37-42.
- 17 Straumanis ME, Kim CD (1965) Phase extent of gallium arsenide determined by the lattice constant and density method. Acta Cryst 19: 256-259.
- 18 Tu KN, Mayer JW, Feldman LC (1992) Electronic thin film science. For electrical engineers and Materials Scientists. Macmillan Publishing Company.
- 19 Dunstan DJ (1996) Mathematical model for strain relaxation in multilayer metamorphic epitaxial structures. Phil Mag A 73: 1323-1332.
- 20 Gonzalez D, Araujo D, Aragon G, Garcia R (1997) A work-hardening based model of strain relief in multilayer graded-buffer structures. Appl Phys Lett 71: 3099-3101.